ZnO-based nanostructures for diluted magnetic semiconductor

Millaty MUSTAQIMA, Chunli LIU[*]

Department of Physics, Hankuk University of Foreign Studies, Seoul, South Korea

Abstract: Since the prediction by Dietl et al. in the year 2000, extensive research activities have been focused on the ZnO-based diluted magnetic materials (DMSs). Earlier works were mainly performed using bulk or thin film materials with transition-metal doping, and diverse magnetic properties including ferromagnetism, paramagnetism, and diamagnetism have been reported. Identifying the dominant mechanism of the ferromagnetic ordering and realizing reproducible ferromagnetism above room temperature have been the main research issues, but a consensus is still lacking even today. Recently, reports on ZnO nanostructures with ferromagnetic behavior have been growing due to the novel properties brought about by the high surface-to-volume ratio and surfaces rich in defect states. In this review, we focus primarily on the recent progress in experimental studies of nanostructure ZnO DMSs. We shall separate our discussion into 2 categories as Mn- and Co-doped ZnO and undoped ZnO nanostructures reported in the literature.

Key words: ZnO, diluted magnetic semiconductor, nanostructure, room temperature ferromagnetism

1. Introduction

With the rapid development of microelectronic technology, Moore's law is running out of momentum and researchers are now more poised to exploit the spin property of the electron for better device performance. Spintronics is an emerging technology that exploits the intrinsic spin of the electron in addition to its fundamental electronic charge in solid-state devices [1]. Because spin can be easily manipulated by an external applied magnetic field and has long coherence times, spintronic devices are particularly attractive for storage, magnetic sensors applications, and quantum computing applications. Currently, giant magnetoresistance [2-5] and tunnel magnetoresistance [6] features are mainly used in a class of devices dubbed the spintronics as the physical basis, and they have been applied in commercial hard disk drives very successfully. When combined with semiconductors, more novel spintronic devices are expected to be realized.

It is desirable to fabricate novel and active multifunctional spintronic devices in the realm of semiconductors so that spin-polarized currents can be generated and actively utilized. Additionally, semiconductor-based spintronic devices could be much more easily integrated with traditional semiconductor technology. Therefore, imparting magnetic properties into semiconductors, i.e. through the diluted magnetic semiconductor (DMS) route, is an imperative component of spintronics studies. For successful spintronic applications, 2 criteria must be fulfilled by the DMS materials. First, a relatively high magnetization must be obtained by introducing the magnetic elements in the semiconducting matrix, and second, a ferromagnetic ground state with a Curie temperature (T_c) greatly exceeding room temperature must be realized. However, despite the numerous theoretical and

---

[*]Correspondence: chunliliu@hufs.ac.kr

experimental studies, practical DMS materials with stable and reproducible high-temperature ferromagnetism are still lacking.

One of the most important results in the earlier stages of DMS studies was the demonstration of ferromagnetism in (Ga,Mn)As [7]. The discovery is very attractive because GaAs is a mainstream semiconductor used in lasers, field effect transistors, and other devices. Following this result, the same and many other groups around the world undertook intensive studies on III-V semiconductor-based DMS materials, made significant progress in improving the sample quality, and provided the realm for studying many new physics concepts. However, the Curie temperature of (Ga,Mn)As has not been increased above 180–190 K, and even experts in this field are not very optimistic that a T_c beyond the aforementioned values will be achieved. This limit is set by the Mn concentration. Currently, (Ga,Mn)As is studied more as a model system for studying unique spintronic phenomena and observations that can be applied to other materials later.

Zinc oxide (ZnO) is an inherently n-type II-VI semiconductor with a wide bandgap of 3.30 eV at room temperature (RT) and exhibits a large excitation binding energy of 60 meV. Because of these properties, ZnO produces bright excitonic UV light emission at RT [8–12]. It also presents a high photoconductivity and considerable piezoelectric and pyroelectric behavior [13]. Extensive research activities have been carried out on ZnO in various research areas including semiconductor physics, chemistry, nanotechnology, and interdisciplinary materials science [8–15]. Due to the relatively well-defined doping and defect chemistry, the potential for transparent high-temperature applications, and the ability of lasing spontaneously at ultraviolet wavelengths as compared to other nonoxide II-VI compounds, ZnO was attractive for potential spintronics applications.

An important research area in the realm of ZnO was spawned by the theoretical prediction by Dietl et al. that p-type ZnO doped with Mn would show RT ferromagnetism (RTFM) [16]. Moreover, the prediction was reportedly confirmed by quite a few experimental studies on ZnO doped with a wide range transition metals (TMs) such as Mn, Co, Fe, Cr, Al, Cu, etc. [17–19]. Figure 1 lists the electronic configuration of TM ions. Since n-type ZnO shows a relatively long RT spin-coherence time [20] and it is possible to dope ZnO as either a p- or n-type semiconductor with low resistivity, ZnO has been considered as a realistic option for bipolar spintronics. Both hole- [21–23] and electron-mediated [24–26] ferromagnetism in ZnO DMSs have been reported.

There are many studies reporting the preparation of TM-doped ZnO compounds in the form of thin films or nanostructures via a wide variety of physical and chemical routes, targeting the abovementioned applications. However, the large number of published experimental results is far from being well understood, and there appears no consensus about the origin of the magnetic behavior observed in most cases [27,28]. For nanoscale dimensions, additional effects related to the high surface-to-volume ratio appear, which introduces more complex but also interesting factors in TM-doped ZnO DMS materials. Recent theoretical results predicted an enhancement of hole-mediated magnetization due to the size effect. Peng et al. showed that due to the anisotropic morphology in nanomaterials, the critical hole concentration for stabilizing the magnetization can be much reduced as compared to that needed in bulk materials [29]. This implies that ZnO nanostructures can be a feasible conduit to achieve practical DMS performance.

It should be noted that most of the TM-doped ZnO materials do not order magnetically in well-crystallized bulk forms. For some cases it was demonstrated that the magnetism was due to segregation of metallic clusters [30], while in some systems containing TM elements with different valence states it was attributed to double exchange interaction [31]. The difficulties in explaining the real mechanism of the ferromagnetism observed in TM-doped oxides stimulated an extensive experimental and computational search in recent years for undoped or non-TM doped oxide systems as alternatives to achieve an unambiguous and clean ferromagnetic semiconductor

Metal ions   **3d orbitals**

V^{3+} [Ar]

Cr^{3+} [Ar]

Cr^{2+} [Ar]

Mn^{2+}, Fe^{3+} [Ar]

Fe^{2+}, Co^{3+} [Ar]

Co^{2+} [Ar]

Ni^{2+} [Ar]

Cu^{2+} [Ar]

Cu^{+}, Zn^{2+} [Ar]

Figure 1. Electronic configuration of transition metal ions.

[32,33]. Since the undoped or non-TM doped oxides do not contain ions with partially filled d or f bands, this type of emergent ferromagnetism in undoped oxides has been proposed as 'd^0 ferromagnetism' [34–36]. In conce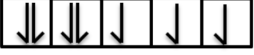rt with the above, recently published works can be divided into 2 categories of TM-doped ZnO or undoped ZnO materials. In most reports, evidence of RTFM is presented together with characterizations aiming to shed some light on the underlying mechanism for the ferromagnetic ordering.

Here we briefly review the recent developments in ZnO-based DMS nanostructures, highlighting the results for Mn-, Co-doped ZnO (ZnO:Mn and ZnO:Co), and undoped ZnO. The experimental results of ZnO-based DMS nanostructures published within the past few years will be reviewed. Earlier results in this field can be found in several other reviews [27,37–39]. Since it is not possible to cover all the published results due to the large numbers of publications, we select some representative works aiming to provide the major issues of the ZnO-based DMS nanostructures.

2. Mn- and Co-doped ZnO nanostructures

Among all the magnetic transition ion-doped ZnO systems, Mn- and Co-doping are usually the most promising systems for the fabrication of spintronic devices mainly because of their abundant electron states and large solubility in the ZnO matrix [40,41]. As indicated by Figure 2, Mn- and Co-doped ZnO nanostructures, judged by the number of the published reports between 2009 and 2014, represent the largest percentage among all the attempted TM elements. It is well known that Mn clusters are antiferromagnetic, so they reduce the net magnetization instead of enhancing the magnetic signal. Additionally, among all oxides of Mn, only MnO is

antiferromagnetic with a Neel temperature of 96 K, and Mn_3O_4 is ferromagnetic with a Curie temperature of 43 K. Therefore, it is not difficult to exclude the effect of Mn clusters or Mn-based oxides from the possible origin of the observed RTFM in ZnO:Mn. Concerning Co-related materials, only metallic Co exhibits high temperature ferromagnetism (T_c = 1400 K) [42]. For most of the reports on ferromagnetic TM-ZnO samples, the research efforts have focused on the identification of the underlying mechanisms through various characterization techniques. Table 1 lists a group of selected experimental results on ZnO:Mn and ZnO:Co from the recent literature.
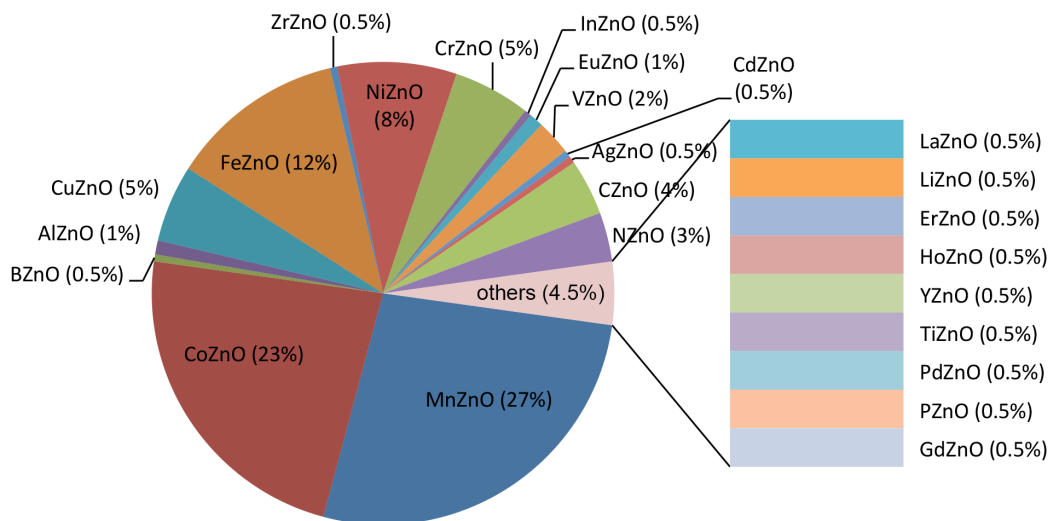

Figure 2. A pie chart showing the percentages of recent publications on ZnO:TM nanostructures.

2.1. Preparation of TM-doped ZnO (ZnO:TM) nanostructures

Most of the ZnO:TM nanostructures, especially nanoparticles, were typically prepared through wet chemical techniques. The chemical precursors employed are zinc acetate $[Zn(CH_3COO)_2 \cdot 2H_2O]$ and acetate of the doping elements, such as manganese acetate $[Mn(CH_3COO)_2 \cdot 4H_2O]$, and potassium hydroxide (KOH) or sodium hydroxide (NaOH) [43–47]. Polymer precursors such as polyvinylpyrrolidone (PVP), polyvinyl alcohol (PVA), ethylene glycol (EG), etc. can be utilized together with acetate precursors to control the morphology [43,48,49].

As illustrated in Figure 3, the typical preparation procedure starts with mixing the metal acetate precursors and potassium hydroxide in an environment of methanol or DI water according to the desired stoichiometry. The mixture is then stirred using a magnetic stirrer at ∼50 °C to obtain a homogeneous solution. After aging for at least 24 h, the precipitates are obtained from the solution. The fine precipitates can be separated by centrifugation and washing repeatedly with distilled water to remove unreacted materials. Finally, the precipitates are dried at ∼100 °C to remove water and annealed at ∼500 °C to get rid of byproducts from the samples. Depending on the doping concentration and preparation conditions, the morphology of the nanostructures can be adjusted or modified [46,49]. Heating and aging can also be performed through hydrothermal process [48] or in a microwave oven using microwave irradiation [45] within a much shorter time (less than 1 h). The wet chemical method is also an facile and flexible approach for the fabrication of hierarchical and self-assembly nanostructures using nanoparticles, nanorods, and nanoplatelets as building blocks [48,50–

Table 1. Overview of the reported experimental results of ZnO:Mn and ZnO:Co nanostructures.

Compound	Doping content x	Fabrication method	Obtained morphology	Magnetic state	Magnetization	Reference
ZnO:Mn	0.028	Chemical vapor deposition (P = ~1000 Pa)	Nanorods	RTFM	0.39 μ_B/Mn	[54]
ZnO:Mn	0.02–0.1	Wet chemical	Nanoparticles	RTFM (x = 0.02 and 0.05) Paramagnetic (x = 0.1)	0.21–0.23 μ_B/Mn (x = 0.02 and 0.05) 0.06 μ_B/Mn (x = 0.1)	[44]
ZnO:Mn	0.03	Microwave-assisted solution route	Nanosheets	RTFM	0.125 emu/g	[45]
ZnO:Mn	0.03	Wet chemical	Nanotubes	RTFM	0.033 emu/g	[46]
ZnO:Mn	0.02–0.07	Hydrothermal	Hierarchical microspheres	RTFM	0.0209 μ_B/Mn (x = 0.02) 0.0144 μ_B/Mn (x = 0.05) 0.0111 μ_B/Mn (x = 0.07)	[48]
ZnO:Mn	0.005–0.06	Hydrothermal method under 4-T magnetic field	Nanocolumns	FM + PM (x = 0.005–0.02) PM (x = 0.06)	~0.006 emu/g (x = 0.005) ~0.0019 emu/g (x = 0.02)	[71]
ZnO:Mn	0.02	Solid-state reaction	N/A	RTFM	0.11 μ_B/Mn	[72]
ZnO:Mn	0.033–0.042	Thermal codissociation in open atmosphere and closed atmosphere	N/A	In open atmosphere: PM In closed atmosphere : FM + PM	4.2 to ~6.0 μ_B/Mn	[73]
ZnO:Mn	0.02	Sol-gel	Nanoparticles	Weak RTFM	~0 to 0.0025 μ_B/Mn	[74]
ZnO:Mn	0.03	Seed-mediated solution	Nanorods	RTFM	0.005 emu/g	[75]
ZnO:Mn	0.02–0.1	Chemical vapor deposition using O_2, Ar, and N_2 as carrier gas	Nanoparticles	RTFM	O_2: ~0.0025 to 0.0125 emu/g Ar: ~0.03 to 0.07 emu/g N_2: ~0.06 to 0.3 emu/g	[76]
ZnO:Mn	0–0.03	Sol-gel	Nanoparticles	PM	0.0321 to ~0.0337 emu/g	[77]
ZnO:Mn	0.02 and 0.05	Aqueous chemical solution	Nanoparticles	RTFM (x = 0.02) PM (x = 0.05)	~0.010 emu/g (RTFM)	[78]
ZnO:Co	≤0.15	Hydrothermal	Flakes	RTFM (x ≤ 0.08) FM+PM (x = 0.1)	0.0118–0.0082 emu/g (x ≤ 0.08)	[79]
ZnO:Co	0.02	Chemical solution	Nanowire	FM at 300 K	0.95 μ_B/Co	[80]
ZnO:Co	0.1	Sol-gel	Nanorods	RTFM	0.13 emu/g at 10 kOe	[81]
ZnO:Co	0.1	Sol-gel	Nanocrystal	RTFM for hydrogenated $Zn_{0.9}Co_{0.1}O$	~0.25 emu/g	[82]
ZnO:Co	~0.036	Vapor-solid process	Y-shape nanostructure	RTFM FM at 400 K	~0.2 emu/g (RTFM) ~0.04 emu/g (at 400 K)	[83]
ZnO:Co	0.08	Vapor transport and Co ion implantation	Nanowire	RTFM	~0.3 μ_B/Co (as-implanted sample) ~0.6 μ_B/Co (3-h vacuum annealing)	[84]
ZnO:Co	0.01–0.05	Sol-gel using PVA as surfactant	Nanorods	Superferromagnetic at RT	0.344–0.483 emu/g	[85]
ZnO:Co	0.03–0.10	Two-step solution route	Nanorods	Weak RTFM at low magnetic field and PM at higher field (<5 mol%) PM (>8 mol%)	N/A	[86]
ZnO:Co	0.05	Sol-gel	Nanoparticles	RTFM	~0.07 emu/g (pure ZnCoO) ~0.08 emu/g (SiO2 treated ZnCoO) ~0.11 emu/g (CNTs treated ZnCoO)	[87]
ZnO:Co	0.03 and 0.05	Ball milling	Nanoparticles	High temperature FM (Tc = 800 K)	3.95 emu/g (x = 0.03) 5.91 emu/g (x = 0.05)	[60]
ZnO:Co	0.05 and 0.15	Solid-state reaction and sol-gel	Bulk (solid-state) Nanoparticles (sol-gel)	Weak ferromagnetic	At 5 K: ~1.7 μ_B/Co (x = 0.05 by solid-state) ~2.4 μ_B/Co (x = 0.05 by sol-gel) ~0.75 μ_B/Co (x = 0.15 by either solid-state or sol-gel)	[88]
ZnO:Co	0.05	Electrophoretic deposition method using anodic aluminum oxide (AAO) as template	Nanowires and nanotubes	RTFM	~0.02 emu/g (nanowires) ~0.04 emu/g (nanotubes)	[89]
ZnO:Co	0.05	Solid-state reaction	Bulk	RTFM, PM	ZnCoO: PM Hydrogenated ZnCoO: 2.9 emu/g ZnCoO (heated for 2 h in air at 550 °C): 0.3 emu/g ZnCoO (heated for 6 h): PM	[90]

52]. Novel or enhanced properties can be obtained in the hierarchical structures through the combination of the building blocks toward targeted applications. In addition to wet chemical approaches, chemical vapor deposition (CVD) [53–55] has also been employed by some research groups to prepare nanostructures with specific morphologies, such as nanotubes or nanorods.
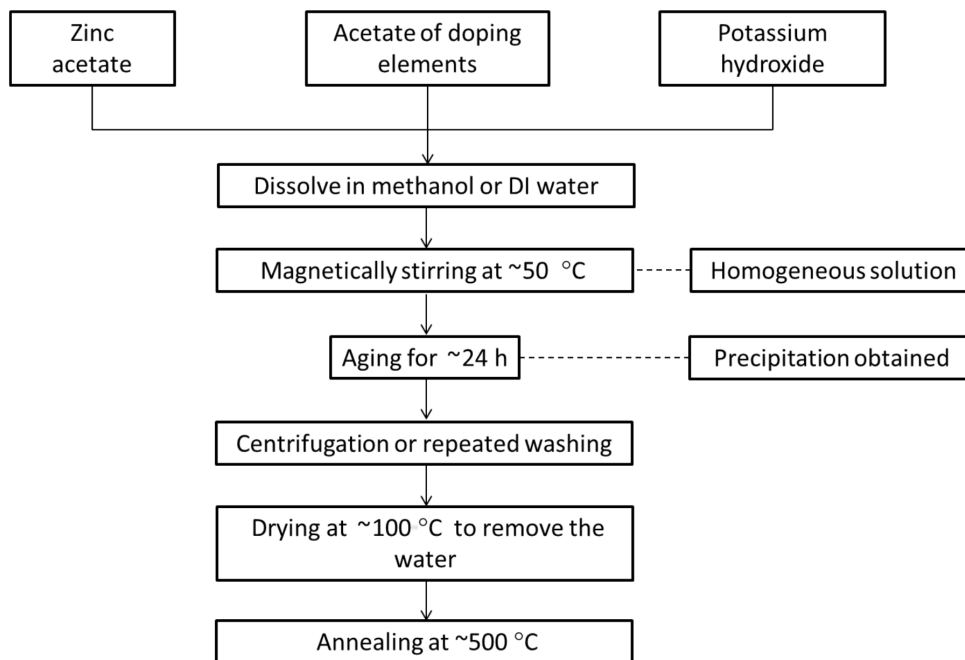

Figure 3. Flow chart showing the typical procedure for the wet chemical preparation of ZnO:TM nanostructures.

2.2. Experimental results on ZnO:Mn and ZnO:Co nanostructures

Although it is desirable to incorporate a large amount of TM ions in the ZnO matrix, formation of clusters of the TM metal or secondary phases must be avoided. The doping concentrations of TM elements employed by most of the research groups are less than 10 mol% to ensure that no secondary peak, corresponding to impurity phases such as the oxides and clusters of Mn and Co, appears in the X-ray diffraction (XRD) spectrum of the samples [43–44,48,49]. XRD provides the preliminary screening of the formation of dopant clusters or secondary phases. Additionally, the shift in the diffraction peak with the increase in TM element content suggests the incorporation of TM ions such as Mn^{2+} ions at the substitutional sites of Zn^{2+} ions.

Further detection of TM impurities and the chemical environment of the ions can be achieved through X-ray photoelectron spectroscopy (XPS) studies. Usually O1s and Mn2p XPS spectra are taken and analyzed using deconvolution with Gaussian–Lorentzian fitting. The typical O1s spectrum shows a peak centered at ~ 530 eV associated with the lattice oxygen (O^{2-}), a peak at ~ 531 eV due to the oxygen in oxygen-deficient regions in the ZnO:Mn matrix [56], and a peak positioned at ~ 532 eV associated with the –OH group [56,57]. For the Mn2p spectrum, the dominant Gaussian peaks are located at about 640.0, 642.6, and 645.0 eV and can be attributed to Mn^{2+}, Mn^{3+}, and Mn^{4+} valence states, respectively [56,58]. The Mn-related peaks on the high-energy side may indicate the existence of Mn impurities such as $ZnMn_2O_4$ or Zn_2MnO_4, which normally cannot be easily detected by XRD due to the minute concentration. The ferromagnetism in ZnO:Mn with 3 at.% doping concentration has been attributed to the double exchange between ZnMnO and Zn-incorporated

Mn-oxide containing Mn^{3+} and/or Mn^{4+} based on the XRD and XPS characterization [46]. For Co ions, the Co-Co bonding is usually located at 778.1–778.3 eV, and the peak corresponding to the Co-O bonding is located around 780 eV [52]. In the XPS spectrum of the Zn 2p core level, the peak positions of Zn 2p3/2 and Zn 2p1/2 are normally located at 1021.9 and 1045 eV, respectively. A spin-orbital splitting of 23.1 eV can be used to confirm that Zn is present as Zn^{2+} [59].

Depending on the growth conditions employed for growing the DMS material, the spatial distribution of TM elements in a nonmagnetic semiconductor can be very different, which will result in different magnetic properties in DMSs. The spatial distribution of TM elements can be characterized using monochromatic cathodoluminescence (CL), as reported in a study of Mn-doped ZnO nanorods prepared by CVD [54]. Comparison of the CL spectra of pure ZnO nanorods and Mn-doped ZnO nanorods revealed that Mn elements are mainly distributed on the surface of Mn-doped ZnO nanorods. The observed RTFM was attributed to the long-range Mn^{2+}–Mn^{2+} ferromagnetic coupling mediated by oxygen vacancies caused by Mn doping.

For most of the reports on ZnO:Mn and ZnO:Co, RTFM was observed in the realm of the magnetic properties. The conclusions proposed for the main factors giving way to the ferromagnetic ordering, however, can be divided as either defect-mediated ferromagnetic coupling or p-d hybridization of the TM ions. In this regard, oxygen annealing can be an effective means to vary the content of oxygen vacancies in the material. Oxygen annealing was employed to study the correlation between the ferromagnetism and the oxygen deficiency in ZnO:Co nanostructures covered with SiO_2 or carbon nanotubes (CNTs) [47]. The results revealed almost no variation of magnetic properties in the SiO_2-covered sample due to the protection by the SiO_2 shell, whereas the ferromagnetism was much reduced by oxygen annealing in samples covered by CNTs due to the filling of oxygen vacancies. The authors concluded that the defect that plays a pivotal role in the enhanced ferromagnetism observed is oxygen vacancy. In addition to oxygen vacancies (the most cited defects for mediating the ferromagnetic ordering), other defects, including zinc interstitials and dislocations, have also been reported to directly affect the RTFM properties in ZnO:TM nanostructures [60–63].

On the other hand, suggestions of RTFM originating from p-d coupling of the TM ions can also be found in the literature. The densities of oxygen interstitials and zinc vacancies were reported to have a direct relation to doping concentration of TM elements, which consequently affects the magnetic properties of the samples [44,46]. Ilyas et al. synthesized ZnO:Mn nanoparticle-based powders with oxygen-rich stoichiometry using a wet chemical method [44]. It was found that the sample with 5 at.% Mn doping showed the maximum saturation magnetization of 0.05 emu/g while having minimum defects as compared to the samples with 2 or 10 at.% Mn doping concentration. Consequently, the authors attributed the ferromagnetic behavior to the strong p-d hybridization of Mn ions instead of oxygen vacancies. The coupling between TM ions usually shows an optimum value at a certain doping concentration, as exhibited by a maximum saturation magnetization of the hysteresis loop. Continuous decrease in the magnetization per Mn ion has been observed in ZnO:Mn hierarchical microspheres with doping concentrations from 2 to 7 at.% [48]. In a study by Duan et al., the maximum saturation magnetization was found in ZnO nanotubes with 3 at.% Mn [46]. For doping concentration higher than 5 at.%, ferromagnetism is usually gradually suppressed by paramagnetic effect with increasing TM concentration [44,46,49,52].

Regarding the optical properties, the following 2 bands often appear in the photoluminescence (PL) spectra: the nearband edge emission (NBE) in the UV region, which originates due to the recombination of free excitons through an exciton–exciton collision process, and the deep level emission (DLE) in the visible region, caused by impurities and structural defects of the crystal. Normally the UV emission is stronger in undoped

ZnO due to the better crystallinity and fewer defects. The increase of the TM elements' concentration leads to the intensity reduction of both UV and blue emissions, which is mainly due to the increase of nonradiative recombination centers induced by TM doping [48,49]. Green emission in DLE can be attributed to the zinc interstitials and oxygen vacancies and also to singly ionized vacancies. The red-orange emissions are attributed to the oxygen interstitials.

Due to the difficulty in achieving reproducible p-type ZnO, codoping with H or N has been pursued by several research groups to achieve hole-mediated ferromagnetic ZnO based on the prediction by Dietl et al. [16]. Codoping of TM elements with excess hydrogen prepared through sol-gel has been used to investigate hydrogen-mediated ferromagnetism [43,64]. Electron paramagnetic resonance (EPR) studies on undoped and ZnO:(H,Mn) powder samples indicated the coupling of the shallow donors to the Mn ions, forming Mn–H_{AB}–Mn complexes as a result, where H_{AB} means stable hydrogen at an antibonding position. Therefore, intentionally incorporated hydrogen as a shallow donor can mediate spin–spin interaction between neighboring Mn^{2+} ions to give rise to RTFM in ZnO:Mn. Furthermore, (Mn,N)-codoped ZnO nanopillars prepared by RF magnetron sputtering showed enhanced RTFM as compared to ZnO:Mn prepared using the same approach [65]. Based on the appearance of acceptors as evidenced from Hall measurement, the ferromagnetism in (Mn,N)-codoped ZnO nanopillars was ascribed to magnetic interaction between the bound magnetic polarons (BMPs) [66–68] formed between the compensated holes generated by N doping and localized magnetic cations created by Mn doping. Besides H or N, codoping with other elements has also been attempted. Jayakumar et al. reported that In doping can dramatically enhance the FM properties in $Zn_{0.95}Co_{0.05}O$ nanoparticles [69], and they attributed the observed enhancement to the additional carriers/defects generated by In codoping.

Regarding the influence of the nanoscale on the ferromagnetic features, there are experimental studies on the saturation magnetization dependency on the crystallite size of nanosized ZnO:Co [60,70]. It was found that the value of saturation magnetization decreases with increasing crystallite size, which was attributed to a decrease in free charge carriers trapped at the grain boundaries. Such variation in turn influences the magnetic ordering in the samples, thereby decreasing the values of saturation magnetization. Similarly, Hu et al. reported that mixing ZnO:Co nanoparticles with SiO_2 nanopowder or CNTs can effectively decrease the particle size and increase the surface area of ZnO:Co nanoparticles, which consequently induce much enhanced magnetization, remnant ratio, and coercivity [47].

3. RTFM in undoped ZnO nanostructures

In addition to TM-doped ZnO, undoped ZnO nanostructures have also been reported to show RTFM even though bulk ZnO is a diamagnetic material. Recent studies on the magnetic properties of pure ZnO nanostructures showed that surface- and defect-states play critical roles in mediating ferromagnetism, despite the lack of definite agreement on the origin and mechanisms. Nanostructures with high surface-to-volume ratio are expected to be an excellent model for studying defect-related ferromagnetism because most of the defects must exist near the surface. Accordingly, it also implies that the RTFM can be tuned by the size of the nanostructures.

For investigating the defect states, PL has often been a useful tool. The effect of defects on the observed magnetic properties of the ZnO nanostructures are often preliminarily characterized through PL. Usually the observed RTFM in ZnO nanostructures can be connected with defects as evidenced from the visible emission in PL [55,97,99]. In particular, the green emission around 520 nm has been attributed to singly occupied oxygen vacancy V_o^+, the yellow emission around 580 nm to doubly charged oxygen vacancy V_o^{2+}, and the orange-red emission to interstitial oxygen O_i on the ZnO surface [91,92,98]. For example, a strong correlation between

the ferromagnetism and the oxygen deficiency in vapor transport-prepared ZnO nanowires has been reported, showing that the highest saturation magnetization was observed in ZnO nanowire with the strongest green emission in PL [97]. The authors therefore proposed that oxygen vacancies boost both the green emission and the magnetism. Imparting a change in defects with annealing conditions is also often used as an effective approach to identify the relation between defects and RTFM. Normally, annealing in oxygen reduces both V_o^+ and V_o^{2+} significantly while increasing the amount of absorbed oxygen at the nanostructure surface and enhances the orange-red emission; annealing in Ar results in a reduction in both green and yellow emission due to the reduction of the surface-captured oxygen and also V_o^{2+}; and annealing in N_2 seems the most effective way for increasing the density of V_o^+ [95,98].

A more detailed identification of the determinant defects can be performed with EPR and XPS. Panigrahy et al. investigated the correlation between defect-related emissions and RTFM of chemically synthesized ZnO nanorods [55]. Based on the EPR and XRS results, the singly charged oxygen vacancies V_O^+ located near the surface were suggested as the main defects that contribute to the RTFM ordering. More recently, a study on ZnO nanoparticles reported similar results regarding the role of V_O^+ [59]. More interestingly, the relative concentration of V_O^+ in both studies can be tuned by the size of the nanoparticles and annealing conditions. Together with similar reports on the size effect [101], it seems clear that size control can be used as one effective approach to tune the magnetic properties in ZnO DMS nanostructures.

As listed in Table 2, a survey of representative recent studies on the RTFM of undoped ZnO nanostructures shows that the oxygen vacancy, and especially V_O^+, has been identified as the dominant defect that directly regulates the FM. Zn vacancies and interstitials have also been proposed to play important roles in determining the magnetic properties in ZnO nanostructures [94,96]. Interestingly, Phan et al. showed that mechanical milling can be used to introduce tremendous amount of defects into ZnO nanoparticles, and based on Raman scattering and electron-spin-resonance measurements Zn vacancies have been suggested as the dominant defect inducing the ferromagnetic ordering [96].

Due to the nanoscale dimension, strong surface effects associated with -H or -OH attachments at the ZnO surface have been found to play an import role in regulating the FM ordering [55,99–101]. The role of surface defects in FM ordering was confirmed by comparing the magnetic properties of ZnO nanowires with different crystallites prepared through CVD and pulse laser vaporization [100]. The authors further argued that the effects of oxygen vacancies and grain size both contribute to the ferromagnetic ordering. Low-temperature (~ 100 °C) annealing of CVD-grown samples in flowing oxygen enhances the ferromagnetic ordering due to an increase in the amount of chemisorbed oxygen, whereas annealing at high temperatures (~ 500 °C), irrespective of the environment, leads to a diamagnetic response due to an increase in the crystal grain size. This report suggested that the ferromagnetic mechanism of the ZnO nanostructure is closely related to the defect states determined by the preparation or treatment conditions.

Overall, the many reports of RTFM in undoped ZnO nanostructures unambiguously state that it is possible to induce ferromagnetic ordering without any TM dopant. The control of the RTFM in undoped ZnO nanostructures, however, does not seem any easier than in the TM-doped ones. It is a must to develop techniques that can effectively regulate the defects and size while maintaining a good enough crystallite of the nanostructures, so that a reproducible RTFM can be achieved.

Table 2. Overview of the reported experimental results of undoped ZnO nanostructures.

Obtained morphology	Fabrication method	Magnetic state	Magnetization	Notes	Reference
Nanorods	Chemical vapor deposition (high temperature)	RTFM	0.031 emu/g	Single ionized oxygen vacancies for BMPs (EPR and PL analysis)	[91]
	Chemical bath deposition (low temperature)		0.06 emu/g		
Nanoparticle pellet	Annealing in oxygen	Diamagnetism		Zn vacancy + OH bonding complex results in a net magnetization	[92]
	Annealing in hydrogen	Weak RTFM	0.7 memu/g		
Nanoparticles	Forced hydrolysis	Weak RTFM	0.2 to ~1.5 meum/g	Zn interstitials and O vacancies induced by annealing enhanced magnetization	[93]
Nanopowder	Mechanical milling and annealing	RTFM	3 memu/g	Zn vacancies at grain surface	[94]
Nanoparticle	Solution route and annealing in N_2, Ar, and O_2	RTFM	1.5 memu/g	Singly ionized oxygen vacancies	[95]
Nanoparticle	Mechanical milling	RTFM		Zinc vacancies	[96]
Nanowire	Vapor transport	RTFM	0.0076 μ_B/Vo	Oxygen vacancies	[97]
Nanowire	Hydrothermal and annealing in Ar and O_2	RTFM	1 memu/g	Singly ionized oxygen vacancies	[98]
Nanoparticles	Wet chemical method	RTFM	1.5 memu/g	Singly ionized oxygen vacancies	[59]
Nanorod array	Hydrothermal and annealing in H_2 and O_2	RTFM	0.15 memu/g	Oxygen vacancies	[99]
Nanowire	Chemical vapor deposition	Weak RTFM	0.2 memu/g	Surface defects and dynamic exchange between O_2 and O_2^-	[100]
	Pulsed laser vaporization	Diamagnetism			
Nanorod	Wet chemical	RTFM	1.5 memu/g	Size effect; singly ionized oxygen vacancies	[55]

4. Summary

We briefly reviewed the recent progress made in magnetic properties in ZnO-related nanostructures. The diversity of experimental results clearly presents the complexity and challenges in this research field. For transition metal Mn- and Co-doped ZnO nanostructures, although most of the works reported the observation of RTFM, diverse factors including uniformly doped host ions and defects induced by dopants are suggested to be responsible for the long-range ferromagnetic ordering. In the case of undoped ZnO nanostructures, although singly charged oxygen vacancy has been most proposed as the dominant defect that boosts the magnetic moment, Zn vacancies and interstitials and defects near the grain boundaries and surfaces have also been shown to be important. Considerable efforts are still necessary in developing an easy and robust strategy to induce a stable and sufficiently strong RTFM in ZnO-related nanostructures with or without transition metal dopants, not to mention that successful operation of a spintronic device requires well controlled spin-polarized transport and detection of spin-polarized current.

Acknowledgment

References

[1] Fiederling, R.; Keim, M.; Reuscher, G.; Ossau, W.; Schmidt, G.; Waag, A.; Molenkamp, L. W. *Nature* **1999**, *402*, 787–790.

[2] Baibich, M. N.; Broto, J. M.; Fert, A.; Van Dau, F. N.; Petroff, F.; Etienne, P.; Creuzet, G.; Friederich, A.; Chazelas, J. *Phys. Rev. Lett.* **1988**, *61*, 2472–2475.

[3] Binasch, G.; Grünberg, P.; Saurenbach, F.; Zinn, W. *Phys. Rev. B* **1989**, 39, 4828–4830.

[4] Barnaś, J.; Fuss, A.; Camley, R. E.; Grünberg, P.; Zinn, W. *Phys. Rev. B* **1990**, *42*, 8110–8120.

[5] Barnaś, J.; Fert, A.; Gmitra, M.; Weymann, I.; Dugaev, V. K. *Phys. Rev. B* **2005**, *72*, 024426.

[6] Moodera, J. S.; Kinder, L. R.; Wong, T. M.; Meservey, R. *Phys. Rev. Lett.* **1995**, *74*, 3273–3276.

[7] Ohno, H. *Science* **1998**, *281*, 951–956.

[8] Tang, Z. K.; Wong, G. K. L.; Yu, P.; Kawasaki, M.; Ohtomo, A.; Koinuma, H.; Segawa, Y. *Appl. Phys. Lett.* **1998**, *72*, 3270–3272.

[9] Bilecka, I; Elser, P.; Niederberger, M. *ACS Nano* **2009**, *3*, 467–477.

[10] Qurashi, A.; Tabet, N.; Faiz, M.; Yamzaki, T. *Nanoscale Res. Lett.* **2009**, *4*, 948–954.

[11] Chen, H.; Wu, X.; Gong, L.; Ye, C.; Qu, F.; Shen, G. *Nanoscale Res. Lett.* **2010**, *5*, 570–575.

[12] Dhara, S.; Giri, P. K. *Nanoscale Res. Lett.* **2011**, *6*, 504.

[13] Wang, Z. L.; Song, J. *Science* **2006**, *312*, 242–246.

[14] Balti, I.; Mezni, A.; Dakhlaoui-Omrani, A.; Leone, P.; Viana, B.; Brinza, O.; Smiri, L.; Jouini, N. *J. Phys. Chem. C* **2011**, *115*, 15758–15766.

[15] Wang, X.; Zheng, R. K.; Liu, Z.; Ho, H.; Xu, J.; Ringer, S. P. *Nanotechnology* **2008**, *19*, 455702.

[16] Dietl, T.; Ohno, H.; Matsukura, F.; Cibert, J.; Ferrand, D. *Science* **2000**, *287*, 1019–1022.

[17] Radovanovic, P. V.; Gamelin, D. R. *Phys. Rev. Lett.* **2003**, *91*, 157202.

[18] Schwartz, D. A.; Gamelin, D. R. *Adv. Mater.* **2004**, *16*, 2115–2119.

[19] Baik, J. M.; Lee, J. L. *Adv. Mater.* **2005**, *17*, 2745–2748.

[20] Ghosh, S.; Sih, V.; Lau, W. H.; Awschalom, D. D.; Bae, S. Y.; Wang, S.; Vaidya, S.; Chapline, G. *Appl. Phys. Lett.* **2005**, *86*, 232507.

[21] Kittilstved, K. R.; Norberg, N. S.; Gamelin, D. R. *Phys. Rev. Lett.* **2005**, *94*, 147209.

[22] Lim, S. W.; Jeong, M. C.; Ham, M. H.; Myoung, J. M. *Jpn. J. Appl. Phys.* **2004**, *43*, L280–L283.

[23] Norberg, N. S.; Kittilstved, K. R.; Amonette, J. E.; Kukkadapu, R. K.; Schwartz, D. A.; Gamelin, D. R. *J. Am. Chem. Soc.* **2004**, *126*, 9387–9398.

[24] Saeki, H.; Tabata, H.; Kawai, T. *Solid State Commun.* **2001**, *120*, 439–443.

[25] Schwartz, D. A.; Gamelin, D. R. *Adv. Mater.* **2004**, *16*, 2115–2119.

[26] Venkatesan, M.; Fitzgerald, C. B.; Lunney, J. G.; Coey, J. M. D. *Phys. Rev. Lett.* **2004**, *93*, 177206.

[27] Liu, C.; Yun, F.; Morkoc, H. *J. Mater. Sci.-Mater. El.* **2005**, *16*, 555–597.

[28] Avrutin, V.; Izyumskaya, N.; Özgür, U.; Silversmith, D. J.; Morkoç, H. *Proc. IEEE.* **2010**, *98*, 1288–1301.

[29] Peng, H.; Xiang, H. J.; Wei, S. H.; Li, S. S.; Xia, J. B.; Li, J. B. *Phys. Rev. Lett.* **2009**, *102*, 017201.

[30] Shinde, S. R.; Ogale, S. B.; Higgins, J. S.; Zheng, H.; Millis, A. J.; Kulkarni, V. N.; Ramesh, R.; Greene, R. L.; Venkatesan, T. *Phys. Rev. Lett.* **2004**, *92*, 166601.

[31] Kittilstved, K. R.; Gamelin, D. R. *J. Am. Chem. Soc.* **2005**, *127*, 5292–5293.

[32] Kittilstved, K. R.; Norberg, N. S.; Gamelin, D. R. *Phys. Rev. Lett.* **2005**, *94*, 147209.

[33] Rubi, D.; Fontcuberta, J.; Calleja, A.; Aragones, Ll.; Capdevila, X. G.; Segarra, M. *Phys. Rev. B.* **2007**, *75*, 155322.

[34] Coey, J. M. D. *Solid State Sci.* **2005**, *7*, 660–667.

[35] Coey, J. M. D.; Stamenov, P.; Gunning, R. D.; Venkatesan, M.; Paul, K. *New J. Phys.* **2010**, *12*, 053025.

[36] Coey, J. M. D.; Kwanruthai, W.; Alaria, J.; Venkatesan, M. *J. Phys. D Appl. Phys.* **2008**, *41*, 134012.

[37] Furdyna, J. K. *J. Appl. Phys.* **1998**, *64*, R29–R64.

[38] Ohno, H.; Munekata, H.; von Molnár, S.; Chang, L. L. *J. Appl. Phys.* **1991**, *69*, 6103–6108.

[39] Pearton, S. J.; Abernathy, C. R.; Overberg, M. E.; Thaler, G. T.; Norton, D. P.; Theodoropoulou, N.; Hebard, A. F.; Park, Y. D.; Ren, F.; Kim, J. et al. *J. Appl. Phys.* **2003**, *93*, 1–13.

[40] Fukumura, T.; Jin, Z.; Ohtomo, A.; Koinuma, H.; Kawasaki, M. *Appl. Phys. Lett.* **1999**, *75*, 3366–3368.

[41] Ueda, K.; Tabata, H.; Kawai, T. *Appl. Phys. Lett.* **2001**, *79*, 988–990.

[42] Kim, J. H.; Kim, H.; Kim, D.; Ihm, Y. E.; Choo, W. K. *J. Appl. Phys.* **2002**, *92*, 6066–6071.

[43] Park, J. K.; Lee, K. W.; Kweon, H.; Lee, C. E. *Appl. Phys. Lett.* **2011**, *98*, 102502.

[44] Ilyas, U.; Rawat, R. S.; Tan, T. L.; Lee, P.; Chen, R.; Sun, H. D.; Fengji, L.; Zhang, S.; *J. Appl. Phys.* **2012**, *111*, 033503.

[45] Ahmed, F.; Kumar, S.; Arshi, N.; Anwar, M. S.; Heo, S. N.; Koo, B. H. *Acta Mater.* **2012**, *60*, 5190–5196.

[46] Duan, J.; Wang, H.; Wang, H.; Zhang, J.; Wu, S.; Wang, Y. *CrystEngComm* **2012**, *14*, 1330–1336.

[47] Gu, H.; Zhang, W.; Xu, Y.; Yan, M. *Appl. Phys. Lett.* **2012**, *100*, 202401.

[48] Hao, Y. M.; Lou, S. Y.; Zhou, S. M.; Yuan, R. J.; Zhu, G. Y.; Li, N. *Nanoscale Res. Lett.* **2012**, *7*, 100.

[49] Kaur, J.; Kotnala, R. K.; Gupta, V.; Verma, K. C. *Current Appl. Phys.* **2014**, *14*, 749–756.

[50] Zeng, X.; Yuan, J.; Zhang, L. *J. Phys. Chem. C* **2008**, *112*, 3503–3508.

[51] Barick, K. C.; Aslam, M.; Dravid, V. P.; Bahadur, D. *J. Phys. Chem. C* **2008**, *112*, 15163–15170.

[52] Hao, H.; Qin, M.; Li, P. *J. Alloy. Compd.* **2012**, *515*, 143–148.

[53] Zhang, X. M.; Mai, W.; Zhang, Y.; Ding, Y.; Wang, Z. L. *Solid State Commun.* **2009**, *149*, 293–296.

[54] Yan, H. L.; Wang, J. B.; Zhong, X. L.; Zhou, Y. C. *Appl. Phys. Lett.* **2008**, *93*, 142502.

[55] Panigrahy, B.; Aslam, M.; Misra, D. S.; Ghosh, M.; Bahadur, D. *Adv. Funct. Mater.* **2010**, *20*, 1161–1165.

[56] Li, J. H.; Shen, D. Z.; Zhang, J. Y.; Zhao, D. X.; Li, B. S.; Lu, Y. M.; Liu, Y. C.; Fan, X. W. *J. Magn. Magn. Mater.* **2006**, *302*, 118–121.

[57] Deshmukh, A. V.; Patil, S. I.; Yusuf, S. M.; Rajarajan, A. K.; Lalla, N. P. *J. Magn. Magn. Mater.* **2010**, *322*, 536–541.

[58] Singhal, R. K.; Dhawan, M. S.; Gaur, S. K.; Dolia, S. N.; Kumar, S.; Shripathi, T.; Deshpande, U. P.; Xing, Y. T.; Saitovitch, E.; Garg, K. B. *J. Alloy. Compd.* **2009**, *477*, 379–385.

[59] Xu, X.; Xu, C.; Dai, J.; Hu, J.; Li, F.; Zhang, S. *J. Phys. Chem. C* **2012**, *116*, 8813–8818.

[60] Pal, B.; Giri, P. K. *J. Appl. Phys.* **2010**, *108*, 084322.

[61] Djerdj, I.; Jagličić, Z.; Arčon, D.; Niederberger, M. *Nanoscale* **2010**, *2*, 1096–1104.

[62] Zhang, Z. H.; Tao, H. L.; Pan, L. L.; Gu, L.; He, M.; Song, B.; Li, Q. *Scripta Mater.* **2013**, *69*, 262–265.

[63] Zhang, Z. H.; Wang, X. F.; Xu, J. B.; Muller, S.; Ronning, C.; Li, Q. *Nat. Nano.* **2009**, *4*, 523–527.

[64] Lee, S. H.; Cho, Y. C.; Kim, S. J.; Cho, C. R.; Jeong, S. Y.; Kim, S. J.; Kim, J. P.; Choi, Y. N.; Sur, J. M. *Appl. Phys. Lett.* **2009**, *94*, 212507.

[65] Wang, D. D.; Xing, G. Z.; Yan, F.; Yan, Y. S.; Li, S. *Appl. Phys. Lett.* **2014**, *104*, 022412.

[66] Kaminski, A.; Sarma, S. D. *Phys. Rev. Lett.* **2002**, *88*, 247202.

[67] Liu, C.; Yun, F.; Morkoc, H. *J. Mater. Sci.-Mater. El.* **2005**, *16*, 555–597.

[68] Xu, H. Y.; Liu, Y. C.; Xu, C. S.; Liu, Y. X.; Shao, C. L.; Mu, R. *Appl. Phys. Lett.* **2006**, *88*, 242502.

[69] Jayakumar, O. D.; Sudakar, C.; Persson, C.; Salunke, H. G.; Naik, R.; Tyagi, A. K. *Appl. Phys. Lett.* **2010**, *97*, 232510.

[70] Lakshmi, Y. K.; Srinivas, K.; Sreedhar, B.; Raja, M. M.; Vithal, M.; Reddy, P. V. *Mater. Chem. Phys.* **2009**, *113*, 749–755.

[71] Yang, T.; Li, Y.; Zhu, M. Y.; Li, Y. B.; Huang, J.; Jin, H. M.; Hu, Y. M. *Mater. Sci. Eng. B* **2010**, *170*, 129–132.

[72] Chattopadhyaya, S.; Neogi, S. K.; Sarkar, A.; Mukadam, M. D.; Yusuf, S. M.; Banerjeea, A.; Bandyopadhyay, S. *J. Magn. Magn. Mater.* **2011**, *323*, 363–368.

[73] El-Hilo, M.; Dakhel, A. A. *J. Magn. Magn. Mater.* **2011**, *323*, 2202–2205.

[74] Sharma, V. K.; Ojha, N.; Varma, G. D. *J. Phys. Chem. Solids* **2009**, *70*, 941–947.

[75] Wang, H. B.; Wang, H.; Zhang, C.; Yang, F. J.; Duan, J. X.; Yang, C. P.; Gu, H. S.; Zhou, M. J.; Li, Q.; Jiang, Y. *J. Nanosci. Nanotechno.* **2009**, *9*, 3308–3312.

[76] Sharma, V. K.; Najim, M.; Srivastava, A. K.; Varma, G. D. *J. Magn. Magn. Mater.* **2012**, *324*, 683–689.

[77] Moontragoon, P.; Pinitsoontorn, S.; Thongbai, P. *Microelectron. Eng.* **2103**, *108*, 158–162.

[78] Wang, Z. H.; Geng, D. Y.; Zhang, Z. D. *Solid State Comm.* **2009**, 149, 682–684.

[79] Xu, X.; Cao, C. *J. Alloys and Compounds* **2010**, *501*, 265–268.

[80] Yao, T.; Yan, W.; Sun, Z.; Pan, Z.; Xie, Y.; Jiang, Y.; Ye, Y.; Hu, F.; Wei, S. *J. Phys. Chem. C* **2009**, *113*, 14114–14118.

[81] Maensiri, S.; Laokul, P.; Klinkaewnarong, J.; Thomas, C. *Appl. Phys. A* **2009,** *94*, 601–606.

[82] Lee, S.; Cho, Y. C.; Kim, S. J.; Cho, C. R.; Jeong, S. Y.; Kim, S. J.; Kim, J. P.; Choi, Y. N.; Sur, J. M. *Appl. Phys. Lett.* **2009**, *94*, 212507.

[83] Zhang, X. M.; Mai, W.; Zhang, Y.; Ding, Y.; Wang, Z. L. *Solid State Comm.* **2009**, *149*, 293–296.

[84] Chen, I. J.; Ou, Y. C.; Wu, Z. Y.; Chen, F. R.; Kai, J. J.; Lin, J. J.; Jian, W. B. *J. Phys. Chem. C* **2008**, *112*, 9168–9171.

[85] Kaur, J.; Kotnala, R. K.; Gupta, V.; Verma, K. C. *Current Appl. Phys.* **2014**, *14*, 749–756.

[86] Hao, H.; Qin, M.; Li, P. *J. Alloy. Compd.* **2012**, *515*, 143–148.

[87] Gu, H.; Zhang, W.; Xu, Y.; Yan, M. *Appl. Phys. Lett.* **2012**, *100*, 202401.

[88] Vagadia, M.; Ravalia, A.; Khachar, U.; Solanki, P. S.; Doshi, R. R.; Rayaprol, S.; Kuberkar, D. G. *Mater. Res. Bul.* **2011**, *46*, 1933–1937.

[89] Jun, L. J.; Ting, Z. L.; Bo, Z. J.; Yin, L.; Chang, H. W. *T. Nonferr. Metal Soc.* **2012**, *22*, 95–99.

[90] Singhal, R. K.; Samariya, A.; Xing, Y. T.; Kumar, S.; Dolia, S. N.; Deshpande, U. P.; Shripathi, T.; Saitovitch, E. B. *J. Alloy. Compd.* **2010**, *496*, 324–330.

[91] Xu, X.; Xu, C; Lin, Y.; Li, J.; Hu, J. *J. Phys. Chem. C* 2013, *117*, 24549–24553.

[92] Xue, X.; Liu, L.; Wang, Z.; Wu, Y. *J. Appl. Phys.* **2014**, *115*, 033902.

[93] Rainey, K.; Chess, J.; Eixenberger, J.; Tenne, D. A.; Hanna, C. B.; Punnoose, A. *J. Appl. Phys.* **2014**, *115*, 17D727.

[94] Ghose, S.; Sarkar, A.; Chattopadhyay, S.; Chakrabarti, M.; Das, D.; Rakshit, T.; Ray, S. K.; Jana, D. *J. Appl. Phys.* **2013**, *114*, 073516.

[95] Liu, W.; Li, W.; Hu, Z.; Tang, Z.; Tang, X. *J. Appl. Phys.* **2011**, *110*, 013901.

[96] Phan, T. L.; Zhang, Y. D.; Yang, D. S.; Nghia, N. X.; Thanh, T. D.; Yu, S. C. *Appl. Phys. Lett.* **2013**, *102*, 072408.

[97] Xing, G. Z.; Wang, D. D.; Yi, J. B.; Yang, L. L.; Gao, M.; He, M.; Yang, J. H.; Ding, J.; Sum, T. C.; Wu, T. *Appl. Phys. Lett.* **2010**, *96*, 112511.

[98] Kushwaha, A.; Tyagi, H.; Aslam, M. *AIP Advances* **2013**, *3*, 042110.

[99] Xu, X.; Xu, C.; Lin, Y.; Ding, T.; Fang, S.; Shi, Z.; Xia, W.; Hu, J. *Appl. Phys. Lett.* **2012**, *100*, 172401.

[100] Podila, R.; Queen, W.; Nath, A.; Arantes, J. T.; Schoenhalz, A. L.; Fazzio, A.; Dalpian, G. M.; He, J.; Hwu, S. J.; Skove, M. J. et al. *Nano Lett.* **2010**, *10*, 1383–1386.

[101] Li, T.; Ong, C. S.; Herng, T. S.; Yi, J. B.; Bao, N. N.; Xue, J. M.; Feng, Y. P.; Ding, J. *Appl. Phys. Lett.* **2011**, *98*, 152505.